Three-Dimensional Vascular Smooth Muscle Orientation as Quantitatively Assessed by Multiphoton Microscopy: Mouse Carotid Arteries Do Show a Helix

Bart Spronck-*EMBS Member*, Remco T.A. Megens, Koen D. Reesink, and Tammo Delhaas

Abstract— **Smooth muscle cells (SMCs) play a pivotal role in regulating vascular tone in arteries, and are therefore an essential part of constitutive models of the artery wall. In the present study, we developed a method to quantify in 3D the orientation of SMCs in the intact artery wall. We stained cell nuclei in excised mouse carotid arteries mounted between micropipettes and imaged these in 3D using two-photon laser scanning microscopy. A clustering method was used to identify individual nuclei. Orientations of these nuclei (as a representative of the SMC orientations) were found by calculating the inertia matrix eigenvectors. Subsequently, SMC locations and orientations were converted to cylindrical and spherical coordinate systems, respectively. We found SMCs to be arranged in two distinct layers. For each of these layers, SMC orientations were described by a Bingham distribution. Distributions showed a statistically significant helical and transversal angular component in both inner and outer layers. In conclusion, this study demonstrates that SMC orientation can be quantified in 3D, and shows a distinct helical as well as transversal orientation. The acquired distribution data are essential to improve current constitutive models of the artery wall, by describing physiological SMC orientation and dispersion.**

I. Introduction

In the arterial system, smooth muscle cells (SMCs) regulate vascular tone. As it is well established that this contribution of SMCs to arterial biomechanics plays an essential role in arterial biomechanics, current constitutive models of the arterial wall include a smooth muscle component [1, 2]. Since SMCs exert their contractile force mainly along their longitudinal axis, SMC orientation is a major determinant of SMC biomechanical behavior. To our knowledge, all current constitutive models assume SMC orientation to be perfectly circumferential, presumably so because experimental studies often describe arterial SMC orientation to be circumferential [3, 4]. However, the main limitation of these experimental studies is that they require fixation of the arteries, potentially introducing artifacts.

In a previous study [5], we developed a 2D method to quantify smooth muscle orientation in vessels (specifically, rat ureters) using two-photon laser scanning microscopy (TPLSM). Using this approach in the mouse carotid artery had its limitations. Firstly, only a very small part of the wall could be analyzed. Secondly, an eventually present transverse angle could not be quantified. Thirdly SMCs appeared to be organized in one, thick layer.

In the present study, we propose an improved method for vascular SMC orientation quantification, analyzing orientation in three dimensions at once. This method allows for the analysis of large datasets and for quantification of transverse angles. We used our approach to assess the SMC orientation in mouse carotid arteries, in an attempt to provide more detailed input data for further biomechanical modeling studies.

II. Materials and Methods

A. Animals and staining

Left common carotid arteries of six male C57/BL6JRJ mice (age: 8 weeks) were excised, labeled at the proximal end, and mounted between micropipettes as described previously [6]. SMC nuclei were stained using 2.7 μM SYTO 13 (Life Technologies) for 30 minutes. Arteries were maximally vasodilated by addition of 10 μM nitroprusside and were kept pressurized at 40 mmHg throughout the experiment. All animal experiments were approved by the local authority.

B. Image acquisition

Imaging was performed using a TPLSM system (Leica TCS SP5II MP, Leica Mikrosysteme Vertrieb GmbH, Wetzlar, Germany) equipped with a Leica HCX APO L 20x/1.00W water dipping objective. Two-photon excitation was achieved using a pulsed Ti-Sapphire laser (Spectra Physics MaiTai DeepSee, Newport, USA) tuned at 825 nm. Signal detection was performed using a descanned detector (GaAsP, Leica HyD) between wavelengths of 510 and 555 nm. Image slices of 1480x1480 pixels were acquired with a voxel size of 0.5x0.5x0.5 μm^3 and a voxel dwell time of 1.1 μs.

Research supported by a Maastricht University Kootstra talent fellowship awarded to B. Spronck.

B. Spronck is with the Department of Biomedical Engineering, CARIM School for Cardiovascular Disease, Maastricht University, Maastricht, The Netherlands (corresponding author, phone +31 43 388 1664; e-mail b.spronck@maastrichtuniversity.nl).

R.T.A. Megens is with the Institute for Cardiovascular Prevention, Ludwig-Maximilians-Universität, Munich, Germany, and with the Department of Biomedical Engineering, CARIM School for Cardiovascular Disease, Maastricht University, Maastricht, The Netherlands (e-mail remco.megens@med.uni-muenchen.de).

K.D. Reesink is with the Department of Biomedical Engineering, CARIM School for Cardiovascular Disease, Maastricht University, Maastricht, The Netherlands (e-mail k.reesink@maastrichtuniversity.nl).

T. Delhaas is with the Department of Biomedical Engineering, CARIM School for Cardiovascular Disease, Maastricht University, Maastricht, The Netherlands (e-mail tammo.delhaas@maastrichtuniversity.nl).

978-1-4244-7929-0/14/$26.00 ©2014 IEEE

C. Image processing

1) Deconvolution and vesselness filtering

Raw image stacks were deconvolved using 10-pass adaptive blind 3D deconvolution (AutoQuant X2, MediaCybernetics, Bethesda, MD). Further data processing and analysis were performed using MATLAB R2013b (MathWorks, Natick, MA). After deconvolution, the deconvolved data stack was 3D vesselness-filtered [7] to enhance elongated structures. Filtering parameters were adjusted to match SMC size and geometry.

2) Clustering and cell orientation calculation

In order to separate cell nuclei from background, the vesselness stack was thresholded at a cut-off value of 0.01. Voxels were then clustered based on their 3D 6-connected neighborhood [8]. Clusters were included based on their volume using upper (320.1 μm^3) and lower (38.5 μm^3) thresholds calculated as mean±2SD from aortic SMC nucleus sizes [9]. An example of a stack of clustered nuclei is given in Fig. 1. For each cluster, an inertia matrix was calculated [10, 11]. The eigenvector corresponding to the largest eigenvalue of this matrix represents the principal SMC orientation.

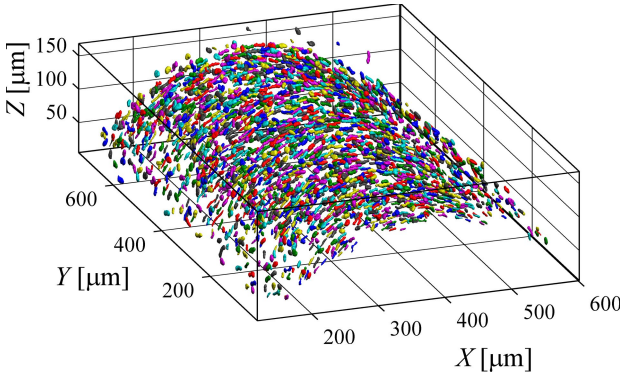

Figure 1. Representative example of segmented SMCs. Colors are randomly assigned to clarify separation between cells.

3) Coordinate transformation

In order to assess SMC orientations with respect to the vessel wall, a cylinder was least-squares fitted through the detected centroids. The cylinder axis was used as a reference to convert all centroid *locations* to cylindrical coordinates (ρ,θ,z, Fig. 2A), rather than Cartesian coordinates (X,Y,Z). The *orientations* of the SMCs were expressed locally with respect to the vessel wall (Fig. 2B), and are represented as a point on a unit hemisphere (Fig. 2C). Orientations are specified by a helix angle (θ_h) and a transverse angle (θ_t).

4) Smooth muscle layer separation

For each sample, cell density was plotted as a function of coordinate ρ, as exemplified in Fig. 3A. Because the SMCs showed to be concentrated in two distinct layers, we chose to analyze SMC orientation separately for the inner and outer layers. Therefore, we detected the two density maxima, the distance between which we defined as 2Δ. Each layer is taken to be centered around its maximum, with boundaries of $\pm\Delta$ on each side (Fig. 3A).

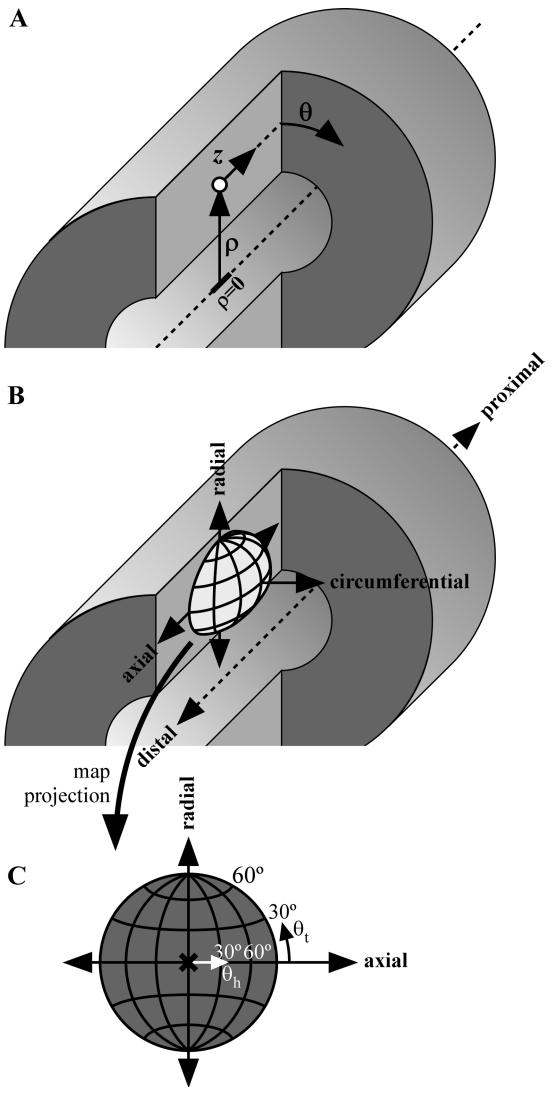

Figure 2. Coordinate system definitions. A: Cylindrical coordinates are used to represent the centers of SMC nuclei. The radial coordinate (ρ) is defined to be 0 at the vessel axis. B: The orientation of a SMC is expressed with respect to the axial, circumferential, and radial coordinate axes, and can be visualized as a position on a unit hemisphere. C: The hemisphere in B is visualized using a map projection (Lambert azimuthal equal-area [12]). The cross denotes a purely circumferential orientation. An orientation can be expressed by two numbers: a helix angle (θ_h) and a transverse angle (θ_t).

5) Orientation (Bingham) statistics

In order to quantify 3D orientation data, directional (spherical) statistics are required [13]. In this case, we are dealing with axial data, i.e., orientations in 3D, which are undirected (an SMC does not have a head or a tail). We chose to describe our data using a Bingham distribution [14, 15]. The five parameters that quantify a Bingham distribution are explained in Fig. 4 and its legend. An example Bingham distribution fitted to a full dataset (non layer-separated) is inset in Fig. 3A.

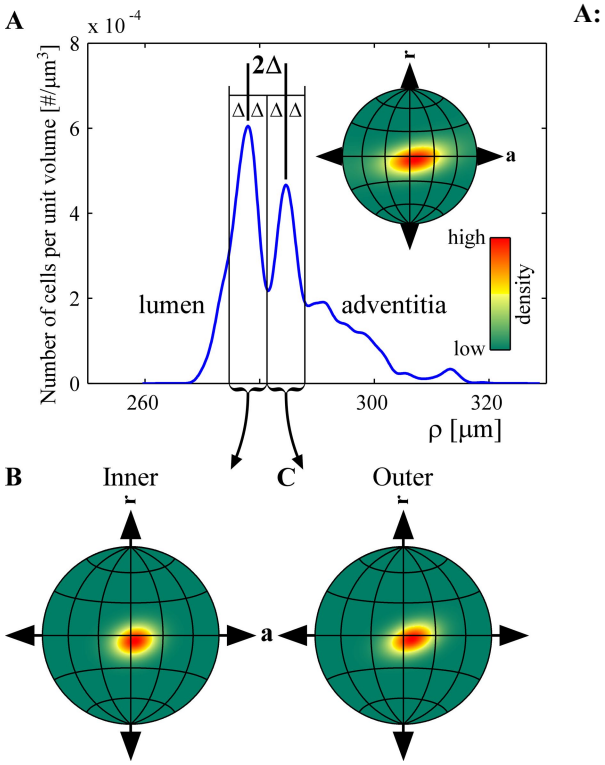

Figure 3. A: Cell density as a function of the radial coordinate (ρ) for a representative sample. SMCs are located in two distinct layers, separated by a distance of 2Δ, as determined by the detected maxima of the density plot. Layer boundaries are subsequently taken at a distance Δ from their density maxima. a: axial, r: radial. Inset: Bingham distribution describing the density of cell orientations for the entire sample. B and C: Bingham distributions fitted to cells in the inner (B) and outer (C) layer.

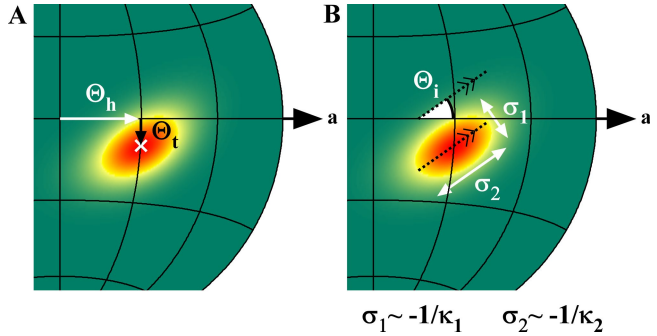

Figure 4. Specification of parameters defining the Bingham distributions. A: Location of the center of gravity, defined using helix angle (Θ_h) and a transverse angle (Θ_t). B: The distribution's spread is, in general, anisotropic and is described by two parameters: κ_1 and κ_2. These are defined to be negative, with $\kappa_1 \leq \kappa_2$. The more negative a κ is, the more concentrated the distribution, as is clearly exemplified in [16]. One could think of κ as $-1/\sigma$ in a normal distribution: as κ gets closer to 0 (i.e., less negative), the distribution gets wider ($\sigma \to \infty$). Θ_i defines the inclination of the principal spread direction (corresponding to κ_2, or σ_2 in the figure) with respect to the axial-circumferential plane. In this example, Θ_h=30°, Θ_t=−10°, κ_1=−30, κ_2=−10, and Θ_i=30°. Density scale bar is printed in Fig. 3A (inset). a: axial.

III. Results

Fig. 3 shows SMC orientation for a representative sample. The separate analysis of the two SMC layers causes the fitted Bingham distributions to become narrower (Figs. 3B and 3C) than the distribution fitted to the entire sample (Fig. 3A, inset). This example shows a distribution of which the center is slightly shifted to the right (positive Θ_h), indicating that, on average, SMCs are helically oriented in this sample. In addition, Θ_t is smaller than 0, indicating a transversal orientation. This means that, on average, SMCs are not perfectly aligned with the vessel wall (axial-circumferential plane).

Fig. 5 shows the center locations for the fitted distributions of all samples for the inner (A) and outer (B) layers. Note that almost all points are in the lower right quadrant of the plots, implying $\Theta_h > 0$ and $\Theta_t < 0$. These values are quantified in Table 1, showing summary statistics for all six arteries. Both coordinates of the distributions' centers of gravity (Θ_h and Θ_t) are significantly different from zero in both layers (all $p<0.05$). This observation shows the presence of a significant helical as well as a transversal angular component in the orientation of SMCs.

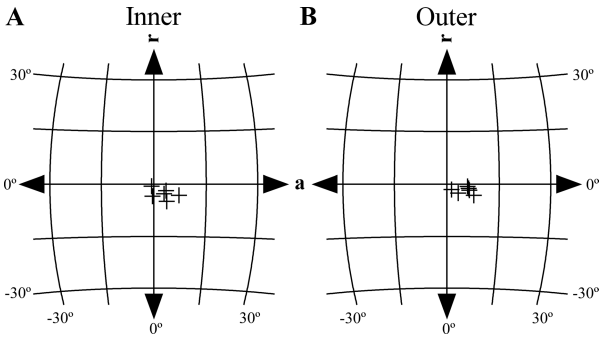

Figure 5. Locations of centers of gravity of the fitted Bingham distributions of all six samples. A and B: Locations for the inner and outer layer, respectively. The mean location of all centers is significantly shifted towards the lower-right quartile of the plot, indicating, on average, nonzero helix and transverse angle.

TABLE I. Summary Bingham Statistics for All Six Carotid Arteries

Parameter	Layer					
	Inner			*Outer*		
κ_1 [-]	−28.9	±	11.3	−35.1	±	12.4
κ_2 [-]	−9.7	±	4.0	−14.0	±	6.5
Θ_h [°]	2.7	±	2.7*	5.1	±	2.2*
Θ_t [°]	−2.8	±	1.3*	−1.8	±	0.8*
Θ_i [°]	9.5	±	5.0*	19.4	±	7.9*,#

Mean±SD (κ_1 and κ_2) or circular mean±circular SD (Θ_h, Θ_t, and Θ_i). The fact that Bingham shape parameters κ_1 and κ_2 differ clearly indicates that the spread of the fitted distributions is elongated. Θ_i's of 9.5° and 19.4° indicate that the largest spread direction is somewhat inclined with respect to the axial-circumferential plane, but is mainly in the circumferential direction. Both helix and transverse angles differ significantly from zero, as also visible in Fig. 5. *$p<0.05$, one-sample Rayleigh test vs. angle zero [17, 18]; #$p<0.05$, inner vs. outer layer paired test (Rayleigh test). Shape parameters (κ_1 and κ_2) did not differ significantly between outer and inner layer (paired t-test).

IV. Discussion

In this study, we propose a method to quantify SMC orientation in vascular structures in 3D. We showed that SMCs in murine carotid arteries are arranged in two distinct layers, and that their orientation is helical, as well as transversal. Additionally, we *quantified* the dispersion in SMC orientation.

The coordinate transformation from Cartesian to cylindrical coordinates allowed us to objectively assess the number of SMC layers in the vessel wall. In contrast, in our previous 2D methodology [5], this layer separation was lost.

The orientation results we obtained contest the finding of most studies that SMC orientation is circumferential. Walmsley found a non-significant mean helix angle of −0.2±2.4° [4], in contrast to our angles of 2.7±1.1° (inner layer) and 5.1±0.9° (outer layer; mean±SEM). Peters et al. report a "truly circumferential" smooth muscle orientation and an "inconsequential" left- or right-handedness of the helix [3], whereas we found a consistent, significant helix. Holzapfel et al, in their modeling paper in 2002, also analyzed SMC orientation [19]. They implemented a method similar to our previous 2D method [5], but used histologically fixed instead of fresh tissue. Interestingly, Holzapfel et al. *assumed* the SMC orientation distribution to be centered around the circumferential direction, and, with that assumption, found two helices with angles of ±8.4°. The results that we obtained, however, contradict this assumption.

Our finding of an arterial helix has potential implications in the field of constitutive modeling of arteries. Additionally, the fact that SMC orientation shows dispersion may have mechanical implications. An example of the mechanical consequence of the inclusion of structural dispersion in constitutive models is given by the collagen modeling performed by Gasser et al. [20]. They found that, due to the dispersion of collagen, the recruitment of collagen fibers occurs at much lower stretches. In addition, when they excluded dispersion, collagen fibers showed larger-than-physiological rotations before bearing any load. Clearly, such effects also play a role in the modeling of SMC contraction in the arterial wall.

A. Limitations

Our study assumes that the orientation of the SMC nuclei is representative for the orientation of SMCs as a whole; an assumption also made in [3, 4, 19] and based on [21]. We made this assumption because after acquisition, cell nuclei appear separated in contrast to the tightly packed SMC bodies and, therefore, are easier to delineate.

Using a dye that stains cell nuclei causes all cells in the artery wall to be stained. Therefore, non-SMCs (e.g., endothelial cells and fibroblasts) may be included in our analyses. However, by only assessing the distinctly visible, narrow smooth muscle layers, we assume that we have excluded the majority of non-SMCs.

Our current study has only assessed arteries at a single (sub-physiological) pressure of 40 mmHg. In the future, it would be interesting to measure SMC orientation at higher pressures, and also assess the dynamic changes in SMC orientation that might occur with a pressure increase.

V. CONCLUSION

This study demonstrates that SMC orientation can be quantified in 3D, and that SMCs show a distinct helical as well as transversal orientation. These findings give rise to further studies into structure-function relationships in cylindrical elastic and contractile vessels.

REFERENCES

[1] M. A. Zulliger, A. Rachev, and N. Stergiopulos, "A constitutive formulation of arterial mechanics including vascular smooth muscle tone," *Am J Physiol Heart Circ Physiol,* vol. 287, pp. H1335-43, Sep 2004.

[2] I. Masson, H. Beaussier, P. Boutouyrie, S. Laurent, J. D. Humphrey, and M. Zidi, "Carotid artery mechanical properties and stresses quantified using in vivo data from normotensive and hypertensive humans," *Biomech Model Mechanobiol,* vol. 10, pp. 867-82, Dec 2011.

[3] M. W. Peters, P. B. Canham, and H. M. Finlay, "Circumferential alignment of muscle cells in the tunica media of the human brain artery," *Blood Vessels,* vol. 20, pp. 221-33, 1983.

[4] J. G. Walmsley, "Vascular smooth muscle orientation in straight portions of human cerebral arteries," *J Microsc,* vol. 131, pp. 361-75, Sep 1983.

[5] B. Spronck, J. J. Merken, K. D. Reesink, W. Kroon, and T. Delhaas, "Ureter smooth muscle cell orientation in rat is predominantly longitudinal," *PLoS One,* vol. 9, p. e86207, Jan 21 2014.

[6] R. T. Megens, S. Reitsma, P. H. Schiffers, R. H. Hilgers, J. G. De Mey, D. W. Slaaf*, et al.*, "Two-photon microscopy of vital murine elastic and muscular arteries. Combined structural and functional imaging with subcellular resolution," *J Vasc Res,* vol. 44, pp. 87-98, 2007.

[7] A. F. Frangi, W. J. Niessen, K. L. Vincken, and M. A. Viergever, "Multiscale vessel enhancement filtering," *Medical Image Computing and Computer-Assisted Intervention - Miccai'98,* vol. 1496, pp. 130-137, 1998.

[8] R. C. Gonzalez and R. E. Woods, *Digital image processing*, 3rd ed. Upper Saddle River, N.J.: Prentice Hall, 2008.

[9] M. K. O'Connell, S. Murthy, S. Phan, C. Xu, J. Buchanan, R. Spilker*, et al.*, "The three-dimensional micro- and nanostructure of the aortic medial lamellar unit measured using 3D confocal and electron microscopy imaging," *Matrix biology : journal of the International Society for Matrix Biology,* vol. 27, pp. 171-81, Apr 2008.

[10] B. Jähne, *Spatio-temporal Image Processing*. Berlin Heidelberg: Sprinter-Verlag, 1993.

[11] D. Vader, A. Kabla, D. Weitz, and L. Mahadevan, "Strain-induced alignment in collagen gels," *PLoS One,* vol. 4, p. e5902, 2009.

[12] K. V. Mardia and P. E. Jupp, *Directional statistics*. Chichester ; New York: J. Wiley, 2000.

[13] N. I. Fisher, T. Lewis, and B. J. J. Embleton, *Statistical analysis of spherical data*. Cambridge Cambridgeshire ; New York: Cambridge University Press, 1987.

[14] C. Bingham, "Distributions on the Sphere and on the Projective Plane," Yale University, 1964.

[15] C. Bingham, "An antipodally symmetric distribution on the sphere," *The Annals of Statistics,* vol. 2, pp. 1201-1225, 1974.

[16] T. C. Onstott, "Application of the Bingham distribution function in paleomagnetic studies," *Journal of Geophysical Research: Solid Earth (1978–2012),* vol. 85, pp. 1500-1510, 1980.

[17] P. Berens, "CircStat: a MATLAB toolbox for circular statistics," *Journal of Statistical Software,* vol. 31, pp. 1-21, 2009.

[18] J. H. Zar, *Biostatistical analysis*, 5th ed. Upper Saddle River, N.J.: Prentice-Hall/Pearson, 2010.

[19] G. A. Holzapfel, T. C. Gasser, and M. Stadler, "A structural model for the viscoelastic behavior of arterial walls: continuum formulation and finite element analysis," *European Journal of Mechanics-A/Solids,* vol. 21, pp. 441-463, 2002.

[20] T. C. Gasser, R. W. Ogden, and G. A. Holzapfel, "Hyperelastic modelling of arterial layers with distributed collagen fibre orientations," *J R Soc Interface,* vol. 3, pp. 15-35, Feb 22 2006.

[21] P. B. Canham, R. M. Henderson, and M. W. Peters, "Coalignment of the muscle cell and nucleus, cell geometry and Vv in the tunica media of monkey cerebral arteries, by electron microscopy," *J Microsc,* vol. 127, pp. 311-9, Sep 1982.